ACS APPLIED MATERIALS & INTERFACES

Forum Article

www.acsami.org

Triblock Copolymer-Encapsulated Nanoparticles with Outstanding Colloidal Stability for siRNA Delivery

Jian Qian and Xiaohu Gao*

Department of Bioengineering, University of Washington, Seattle, Washington 98195, United States

ABSTRACT: A new generation of siRNA nanocarrier with compact, uniform size and excellent colloidal stability has been developed by combining inorganic nanoparticles with rationally designed triblock copolymers. In contrast to conventional cationic polymers and nanoparticles that often condense oligonucleotides into polydisperse aggregates, our nanoparticle–polymer complexes remain single after loading with siRNA. More importantly, they are highly stable even in complete serum, which fills the gap between in vitro technology development using serum-free (or low percentage serum) cell culture media and downstream in vivo applications. Targeted delivery is achieved in GFP-expressing HeLa cells by functionalizing the siRNA delivery vehicle with an integrin-specific peptide ligand. The GFP positive cell population can be reduced from the original 86 to 60 and 25% for nontargeted and targeted nanoparticle–polymer complexes, respectively. At the nanocarrier concentration for siRNA delivery, virtually no cytotoxicity was detected. Further development and validation of this technology by introducing biodegradable and biocompatible core particles and testing them in lab animals could enable widespread uses of siRNA and potentially lead to clinical translation.

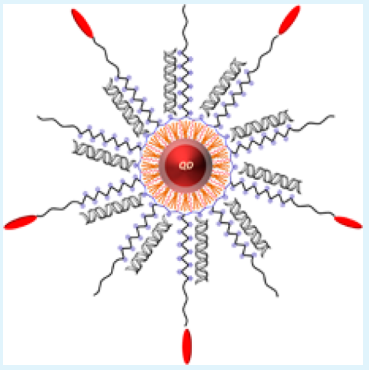

KEYWORDS: *nanoparticles, siRNA delivery, targeting, block copolymer, serum stability*

INTRODUCTION

Short interference RNA (siRNA) is of considerable current interest in biology and medicine because of its capability in probing gene functions and potentially treating tough human diseases.[1−4] Because of the polyanionic and macromolecular characteristics, however, naked siRNA molecules cannot spontaneously cross the cell membrane and thus require delivery vehicles to facilitate cellular uptake and cytosolic release. Toward this goal, substantial progress has been made, in particular for nonviral delivery vectors because they have relatively low immunogenic and oncogenic effects and highly tunable size and surface properties. In recently years, a variety of nanocarries made of cationic lipids, polymers, carbohydrates, inorganic nanoparticles, and their combinations have been developed,[5−10] largely based on complexation or conjugation between siRNA and these carrier materials. When combined with imaging agents, siRNA behaviors in vitro and in vivo such as transport and biodistribution can also be monitored.[8,10−13] For example, we have previously reported the combination of fluorescent quantum dots (QDs) with an amphipol for traceable siRNA delivery and were able to visualize siRNA cell entry, endosome escape, and siRNA-QD dissociation (also known as unpackaging) in real time.[10] The amphipol has clustered tertiary amines with strong proton absorbing capability inside acidic endosomes, leading to osmotic swelling and endosomal escape. Recently, the length and cleavage effects of spacer between QDs and siRNA have also been studied, systematically showing the importance of making cargo siRNA accessible to target mRNA and intracellular enzyme complex.[14]

Despite these recent advances, a common limitation shared by many nanoparticle-based siRNA delivery vehicles is their cationic nature. The positive charges of delivery vehicles are important in condensing negatively charged RNA molecules, preventing siRNA-nanocarrier from premature disassembly, and promoting cell uptake, and are sometimes involved in endosome destabilization. On the other hand, positively charged nanoparticles often result in increased cytotoxicity, nonspecific binding to cells, and in particular low colloidal stability in serum. Upon interaction with ions and serum proteins, electrostatic repulsion can be reduced below van der Waals attraction, which drives aggregate formation. As a result, new siRNA delivery vehicles are routinely developed and evaluated in serum-free cell culture media (even for media containing serum, its concentration is no more than a few percent), which represents a clear disconnect with the in vivo conditions where siRNA complexes are exposed to full blood after intravenous injection.

In this context, we report the rational design of a triblock copolymer that simultaneously achieves inorganic nanoparticle solubilization, siRNA condensation, endosome destabilization, availability of bioconjugation sites, and outstanding colloidal stability in complete serum. To reach this goal, we have prepared

Special Issue: Forum on Biomedical Applications of Colloidal Photoluminescent Quantum Dots

Received: October 1, 2012
Accepted: December 22, 2012
Published: January 15, 2013

   dx.doi.org/10.1021/am3021813 | *ACS Appl. Mater. Interfaces* 2013, 5, 2845−2852

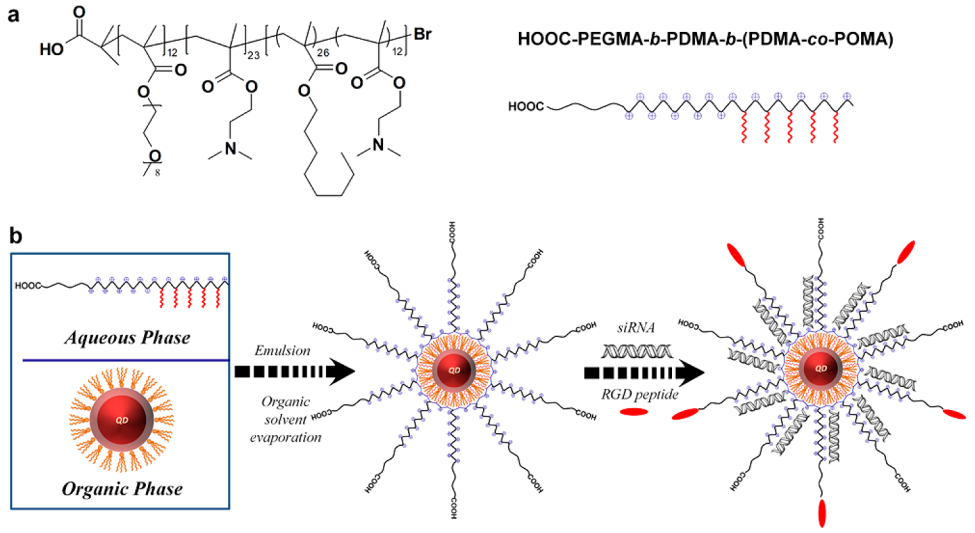

Figure 1. Schematic illustration of the preparation of AB(BC) polymer-encapsulated QDs. (a) Molecular structure of the AB(BC) polymer comprising a hydrophobic block for multivalent binding with hydrophobic nanoparticles, a cationic block for condensing siRNA, and a COOH-terminated PEG block for nanoparticle stabilization. (b) Key steps in AB(BC)-QD self-assembly and functionalization. A microemulsion approach is employed followed by evaporation of the organic solution to drive the QD-polymer self-assembly. The purified nanoparticles are loaded with siRNA cargo molecules through electrostatic interactions and functionalized with peptide targeting ligands for cell selective siRNA delivery.

poly(poly(ethylene glycol) methyl ether methacrylate)-*block*-poly(2-dimethylaminoethyl methacrylate)-*block*-poly(2-dimethylaminoethyl methacrylate-*co*-octyl methacrylate) with a carboxyl group at the terminus of the hydrophilic block (HOOC-PEGMA-*b*-PDMA-*b*-(PDMA-*co*-POMA)). The design features of this multifunctional block polymer are illustrated in Figure 1. Semiconductor QDs are used here as a model inorganic nanoparticle because (i) they serve as a structural scaffold to assemble highly uniform nanocomplexes,[10] (ii) they provide unique optical properties for imaging and tracking,[15,16] and (iii) they share similar surface properties with other types of highly uniform inorganic nanoparticles for broad application and generalization of the technology.[17−19] Instead of adding the functionalities one at a time, the triblock copolymer can self-assemble onto QDs in a single step to achieve all the properties discussed above. Specifically, the hydrocarbons of the hydrophobic PDMA-*co*-POMA block bind with the QD surface ligands (trioctylphosphine oxide or TOPO) through hydrophobic−hydrophobic interactions, whereas the hydrophilic PEGMA and PDMA blocks extend outward and render the entire nanoparticle water-soluble. The PDMA block, with a pK_a of 7.4 and a wide pH buffering zone, serves two functions here. First, in physiological buffers or plasma where the pH value is 7.4, PDMA is approximately 50% protonated.[20] When siRNA molecules are introduced to the nanoparticle carrier, the positively charged PDMA captures siRNA through electrostatic interactions. Second, it has been shown that PDMA is pH-responsive and is capable of disrupting endosome membrane to facilitate drug cytosolic release.[21]

To enhance the colloidal stability of the nanoparticle, the PDMA block is shielded by the PEGMA block as the outer shell. As aforementioned, maintaining the colloidal stability and dispersity in complete serum is critical in efficient drug delivery. This is because size is one of the determining factors for nanoparticle plasma life, blood vessel extravasation, clearance by kidney and the reticuloendothelial systems, and transfer to the lymphatic systems.[22,23] For example, Jiang et al. have reported the nanoparticle size effect on receptor-mediated endocytosis and suggested that ∼50 nm is the optimal size for enhanced cellular uptake.[24] Under *in vivo* conditions, the size effect of nanoparticles becomes even more dramatic, particularly for disease sites with poor permeability. Direct comparison of tumors models with different vascular permeability by Cabral and coworkers shows that sub-100 nm drug-loaded nanoparticles have similar tumor accumulation and treatment effect in hyperpermeable tumor models regardless of nanoparticle size; whereas the size dependency of tumor penetration and therapeutic efficacy in hypopermeable tumors becomes evident.[25] These studies clearly highlight the importance of preventing large aggregate formation and precisely controlling particle size when mixing positively charged siRNA vectors with negatively charged siRNA molecules. Furthermore, the brush-like PEG block also helps reduce the surface charge of the nanoparticle to minimize protein adsorption and opsonization. It has been widely established that nanoparticles with close to neutral surface charges (e.g., based on PEG and zwitterionic coating)[26,27] have the lowest level of protein adsorption.

RESULTS AND DISCUSSION

The block copolymer was synthesized via atom transfer radical polymerization (ATRP). In the first step, PEGMA precursor with a t-butyl ester terminal group was polymerized using CuCl/N,N,N′,N″,N″-pentamethyldiethylenetriamine (PMDETA) as the catalysts and t-butyl 2-bromoisobutyrate as the ATRP initiator. Next, DMA was added and polymerized to reach the desired length of the cationic PDMA block, followed by addition of OMA to form the hydrophobic PDMA-*co*-POMA block. In the polymerization process, ^{1}H NMR was used to monitor the conversion of ethylene glycol methyl ether methacrylate (EGMA) and 2-dimethylaminoethyl methacrylate (DMA). The final structure of AB(BC) block copolymer was confirmed by ^{1}H NMR with the relevant peaks labeled (Figure 2a). In the end, the terminal carboxyl group in the PEGMA block was created by hydrolyzing the t-butyl ester group with hydrochloric acid (6 M). Figure 2b clearly shows that the signal corresponding to the hydrogens of t-butyl group disappeared after conversion to the carboxyl group.

dx.doi.org/10.1021/am3021813 | ACS Appl. Mater. Interfaces 2013, 5, 2845−2852

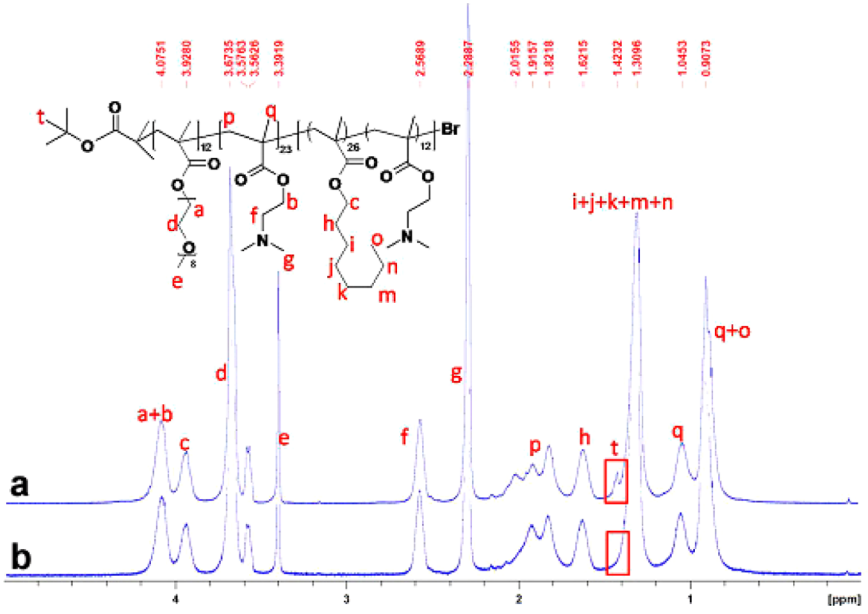

Figure 2. [1]H NMR of AB(BC) block copolymer (a) before and (b) after being treated with hydrochloric acid. The disappearance of peak t (hydrogen signal of t-butyl group) indicates that the t-butyl ester terminal group has been hydrolyzed to carboxyl group.

GPC analysis was also conducted to characterize the size and size distribution of the triblock copolymers. The number average molecular weight (M_n) of PEGMA, PEGMA-PDMA, and PEGMA-PDMA-(PDMA-POMA) are approximately 5900, 10 300, and 15 000 Da, respectively; and the corresponding polydispersity index (PDI, weight average molecular weight divided by number average molecular weight) are 1.29, 1.25, and 1.45.

To test whether the amphiphilic AB(BC) block copolymer can solubilize hydrophobic nanoparticles, we added QDs suspended in chloroform to the polymer aqueous solution. The chloroform–water solvent mixture was sonicated followed by evaporation of the chloroform phase. During this process, the amphiphilic polymer initially serves as the emulsion surfactant, and evaporation of chloroform "drives" it to bind with the hydrophobic QDs through multivalent hydrophobic interactions.[28] The resulting AB(BC) polymer-coated QDs are highly stable in aqueous solution. Their emission peak remains virtually unchanged (Figure 3b) with a fluorescence quantum yield of approximately 30%. This high quantum efficiency is a signature property for QDs solubilized with amphiphilic polymers. For example, previous reports have shown that amphiphilic polymers such as random copolymers, block copolymers, lipid derivatives, and carbohydrate derivatives can encapsulate QDs without replacing their original hydrophobic surface ligands and consequently maintain high quantum efficiency.[29−36] In contrast, ligand exchanged-based QD solubilization approaches often reduce QDs' quantum efficiency dramatically (e.g., >90%).[37] Dynamic light scattering (DLS) measurements show that the AB(BC)-coated QDs have a hydrodynamic diameter of 30 ± 1.5 nm with a polydispersity index of 0.2 (Figure 3c). Considering the core size of QDs is 5.5 ± 0.7 nm in diameter by TEM analysis (Figure 3a), the larger hydrodynamic size in aqueous buffers is likely due to the physical size of the AB(BC) block copolymer, as well as the hydration layer on the nanoparticle surface. For downstream drug delivery applications, we further characterized the siRNA loading capacity of this nanocarrier with gel electrophoresis. To find out the number of siRNA molecules per QD, we incubated FITC-labeled siRNA (green) with QDs emitting red fluorescence at various molar ratios. The quantity of siRNA was set at a fixed value, whereas that of QDs gradually decreased. When the mixture was subject to electrophoretic analysis, siRNA molecules bound to QD surface stayed in the gel loading wells because of the large size of the nanocomplexes, and free (unbound) siRNA was detected based on its characteristic gel mobility and quantified. As shown in Figure 3d, the fluorescence intensity of the siRNA band gradually decreases as QD concentration increases and disappears when the siRNA/QD ratio is below 15, indicating that approximately 15 siRNA molecules can be immobilized onto the surface of individual QDs.

Next, we directly evaluated the colloidal stability of our AB(BC) polymer-encapsulated nanoparticles, the central goal of this work, because it is one of the key factors determining whether nanoparticles are suitable for potential in vivo uses. Please note that the colloidal stability discussed here refers to nanoparticle dispersity in complete serum during the time window of delivery (e.g., hours) rather than resistance to long-term in vivo clearance or enzymatic degradation (e.g., days or months). The stability of AB(BC)-QDs and their siRNA complexes in serum was investigated by quantitative DLS measurements. Although number distribution is more popular in characterizing nanoparticle hydrodynamic sizes in the literature, we chose to use DLS intensity distribution in panels a and b in Figure 4 because it is extremely sensitive in detecting nanoparticle aggregates even though the aggregates represent a much smaller population compared to single particles. This is because large particles are much more effective in scattering light than small particles (the intensity of scattered light by a particle is proportional to the sixth power of its diameter based on Rayleigh scattering approximation). For example, one nanoparticle aggregate of 100 nm will show the same peak area in intensity distribution as that of one million 10 nm single nanoparticles; whereas by number distribution the 100 nm aggregate can be easily overlooked. As shown in Figure 4a, background measurement of 100% serum reveals a bimodal distribution with two peaks centered at ∼10 and 50 nm, which are commonly observed for serum because of the high concentration of proteins.[38]

dx.doi.org/10.1021/am3021813 | ACS Appl. Mater. Interfaces 2013, 5, 2845−2852

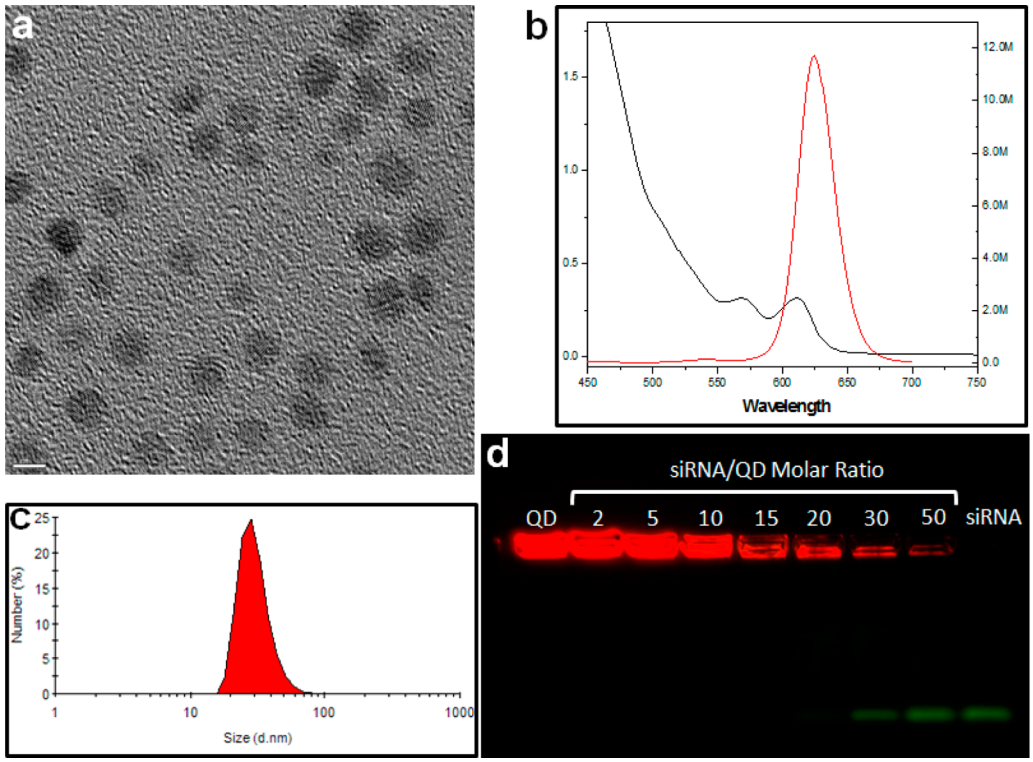

Figure 3. Characterization of the size, optical properties, and siRNA loading capacity of the AB(BC)-QD. (a) QD core size measured by TEM (scale bar 5 nm). (b) Fluorescence absorption and emission profiles of the water-soluble QDs. (c) Hydrodynamic size of a representative QD sample measured by DLS. (d) Determination of siRNA loading capacity on the AB(BC)-QD surface. Twenty pmole of siRNA is mixed with QDs at molar ratios of 2, 5, 10, 15, 20, 30, and 50. Below the ratio of 15, siRNA are completely captured by the nanocarrier (unbound siRNA below the detection sensitivity of gel electrophoresis); whereas higher ratios result in free siRNA in solution.

Addition of AB(BC)-QD and its siRNA complex to serum does not change the DLS spectrum because their sizes are similar to the serum proteins but their concentrations are significantly lower. As a positive control, QDs solubilized with lipid-PEG are also tested in serum because of the outstanding colloidal stability of QD-lipid-PEG. The DLS profiles of QDs solubilized with lipid-PEG and our AB(BC) polymer are virtually the same, and no peaks for large aggregates are observed. In contrast, when cationic amphipol-coated QDs are added to serum (the amphipol does not have a PEG segment),[10] large micrometer-sized aggregates are detected (Figure 4b). We further confirmed the DLS results with fluorescence microscopy. AB(BC)-QD siRNA complex and PEG-lipid-QD in serum (Figure 4c, d) are uniformly spread on glass coverslips and remain single (confirmed by the "blinking" feature) even after 24 h incubation; whereas QDs coated with cationic amphipol become large irregular shaped aggregates in serum (Figure 4e). These studies demonstrated the remarkable stability of AB(BC)-QD in serum, making downstream in vivo applications possible.

The stability can be attributed to the outer PEGMA shell, which eliminates or reduces nonspecific interaction between QDs and serum proteins. Quantitative Zeta potential analysis (Figure 4**f**) reveals that the surface of AB(BC)-QD before siRNA loading is slightly positive (9.3 ± 1.5 mV), indicating that the PEGMA block can mask most of the positive charges of the PDMA block. When siRNA molecules are loaded onto the AB(BC)-QD carriers at 5, 10, and 15 copies of siRNA per nanoparticle, the surface charge further decreases to approximately 5 mV. It has been well documented that close-to-neutral surface of nanoparticles (zeta potential ranged between −10 and +10 mV) can minimize phagocytosis and are less likely to cause immunological reaction in vivo.[39,40] Furthermore, when targeting ligands are linked to nanoparticle surface for cell selective delivery, the PEGylated surface can help improve the targeting specificity, whereas binding of highly positively charged nanoparticles with cells are often dominated by nonspecific electrostatic interactions rather than molecular recognition. This is because most mammalian cells are negatively charged because of the presence of monosaccharides and polysaccharides.

To evaluate the RNAi efficiency using AB(BC)-QD delivery vehicle, we established a model gene silencing experiment using HeLa cells (human cervical cancer) with stable expression of green fluorescent protein (GFP) and siRNA targeting GFP. For targeted delivery, the AB(BC)-QDs are tagged with a Arg-Gly-Asp (RGD) peptide with high affinity and specificity to cell surface integrins, which play important roles in angiogenesis and tumor cell metastasis and have been proposed as therapeutic targets.[41,42] Before the experiment for targeted siRNA delivery was performed, we first confirmed the effect of RGD peptide on AB(BC)-QD cell uptake, as it has been reported in the literature that because of different culturing conditions and passages, HeLa cells may express different levels of integrin receptors.[43−46] Figure 5a clearly shows that the uptake of RGD-targeted QDs by Hela cells is significantly increased compared to the nontargeted QDs. Furthermore, this enhanced cellular uptake can be blocked by addition of free RGD peptides, proving that the enhanced cell uptake is a direct result of the selective binding between the conjugated RGD peptides to the integrins on HeLa cell surface.

To evaluate the siRNA delivery capability of the AB(BC)-QD delivery vehicle, we loaded siRNA targeting GFP onto QD surface and added to the GFP expressing HeLa cells at a siRNA concentration of 80 nM. Figure 5b−d shows the confocal images

dx.doi.org/10.1021/am3021813 | ACS Appl. Mater. Interfaces 2013, 5, 2845−2852

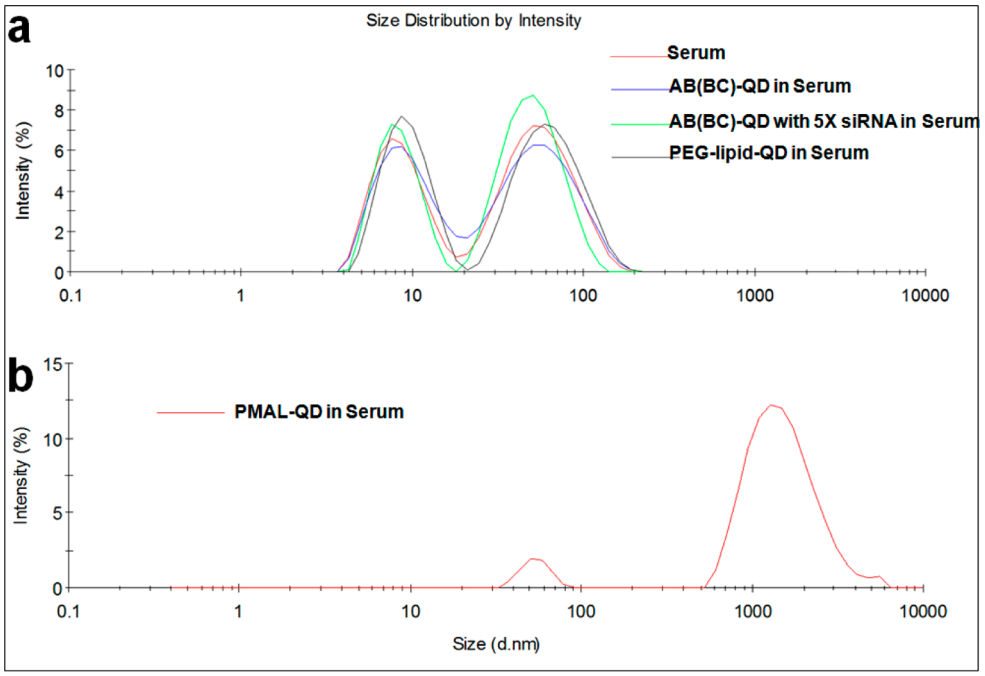

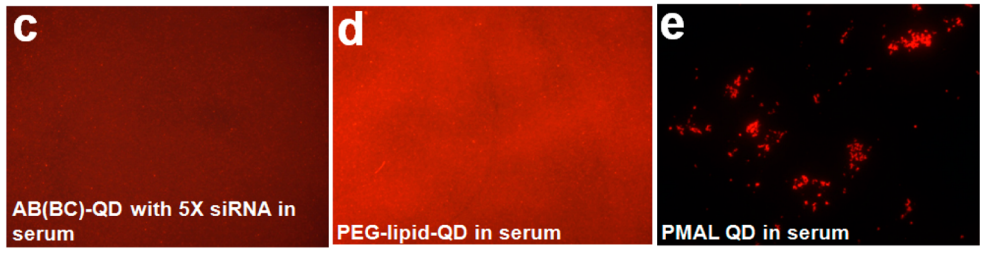

f

siRNA/QD Molar Ratio	0	5	10	15
Zeta Potential	9.3±1.5 mV	5.8±2.5 mV	5.0±2.1 mV	4.5±3.1 mV

Figure 4. Characterization of the colloidal stability and surface charge of the AB(BC)-QD. (a) Hydrodynamic size measurements (intensity distribution) of serum, AB(BC)-QD in serum, AB(BC)-QD with 5X siRNA in serum, and PEG-lipid-QD in serum. Even under intensity weighted presentation, no large aggregates are detected, showing the colloidal stability of the polymer−nanoparticle complexes. (b) The hydrodynamic size of QDs stabilized with a cationic amphipol that we invented previously.[10] Although this cationic nanoparticle is stable in physiological buffers (hydrodynamic size ~15 nm), serum-free media and media with a low percentage of serum, it is not stable in complete serum, indicated by the micrometer-sized aggregate peak. (c−e) Microscopy confirmation of the colloidal stability of AB(BC)-QDs with 5X siRNA, PEG-lipid-QDs, and cationic QDs in serum. Both AB(BC) and PEG-lipid share a similar PEG block, which makes QDs stable in complex biological solutions, as indicated by the uniform spread of nanoparticle layers on coverslips (QD blinking was easily detectable by eye on microscope). In contrast, the cationic QDs without a PEG outer layer precipitate out as irregular shaped aggregates. (f) Zeta potential analysis of AB(BC)-QD before and after loading with siRNA at different ratios.

of the GFP-HeLa cells treated with QD-siRNA complexes and RGD-QD-siRNA complexes. Qualitatively, it appears that the high uptake efficiency of RGD-QD-siRNA (the red fluorescence channel, upper right panel) is directly correlated with the gene silencing efficiency (the green fluorescence channel, upper left panel), whereas the nontargeted QD-siRNA complexes lead to less cell uptake and lower level of GFP expression suppression. The gene-silencing efficiency and nanoparticle cell uptake are further quantitatively assessed by fluorescence-activated cell sorting (FACS), where cells are evaluated with respect to the untreated GFP expressing cells (Figure 5e). At the current gate value set for the GFP fluorescence intensity, the original untreated cells show a GFP-positive population of 86.1%, and the nontargeted QD-siRNA complexes reduce the eGFP-positive population to 59.7%, Figure 5g). Remarkably, when the RGD targeted QD-siRNA complex is applied, the GFP-positive cell group is reduced to 24.8% (Figure 5h), which represents an approximately 60% and 35% drop compared to the original cells and nontargeted treatment group, respectively. From the flow cytometry dot plots, it is clear that higher QD uptake (average intensity on the Y axis) is correlated with lower GFP expression (average intensity on the X axis), but linear relationship between QD uptake and silencing on the individual cell level was not established. Furthermore, as shown in Figure 5i, the silencing effect is also sequence specific as RGD-QD loaded with a random siRNA sequence results in virtually no effect on GFP expression.

Lastly, the cytotoxicity of the AB(BC)-QD carrier was evaluated using the CellTiter-Blue assay. As shown in Figure 6, there was no significant cytotoxicity associated with intracellular accumulation of AB(BC)-QDs even at much elevated nano-

dx.doi.org/10.1021/am3021813 | ACS Appl. Mater. Interfaces 2013, 5, 2845−2852

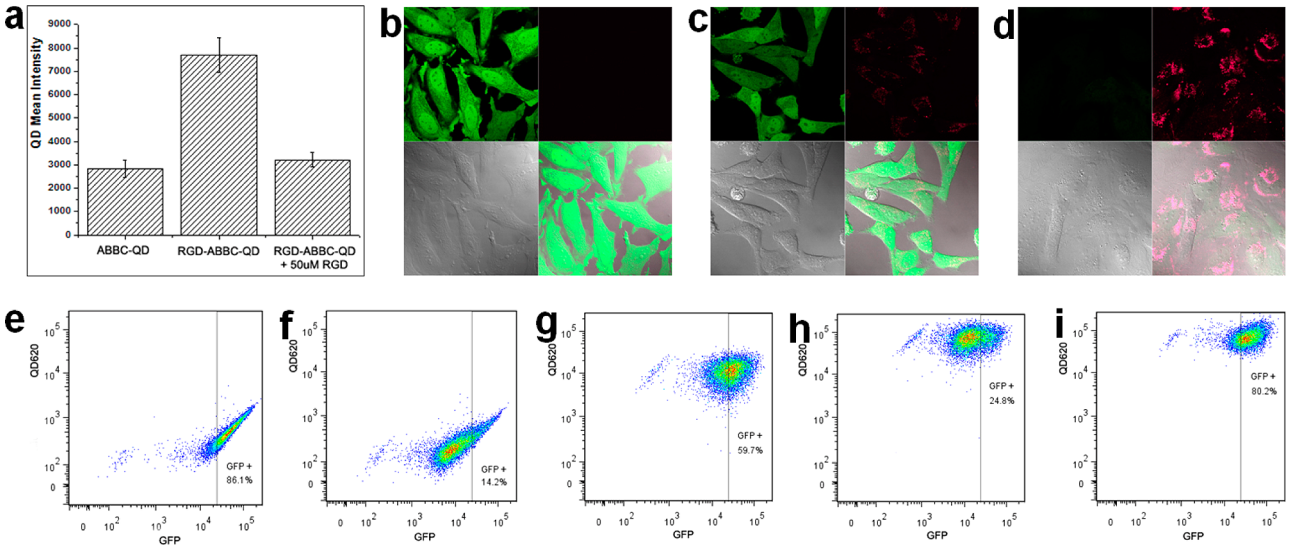

Figure 5. Evaluation of GFP knockdown in GFP-expressing HeLa cells with confocal microscopy and flow cytometry. (a) Confirmation of integrin expression on HeLa cell surface by measuring QD uptake. Mean intensity of HeLa cells treated with AB(BC)-QD, RGD-AB(BC)-QD, and RGD-AB(BC)-QD with 50uM RGD peptides for 5 h clearly demonstrated the effect of RGD peptide. It significantly promotes QD cellular uptake. (b–d) Confocal microscopy of GFP expressing HeLa cells without treatment (negative control), treated with AB(BC)-QD siRNA (80 nM), and with RGD-AB(BC)-QD siRNA (80 nM, positive control), respectively. The fluorescence images show qualitative correlation between the QD uptake and GFP knockdown (the more QD uptake, the lower the GFP expression level). (e–i) Quantitative flow cytometry study of GFP silencing in GFP-expressing HeLa cells, cells treated with Lipofectamine siRNA (80 nM) as positive control, with AB(BC)-QD siRNA (80 nM, negative control), with RGD-AB(BC)-QD siRNA (80 nM), and with RGD-AB(BC)-QD-siRNA (random sequence, 80 nM, negative control). At the current gate value, the GFP-positive populations are 86.1, 14.2, 59.7, 24.8, and 80.2%, respectively.

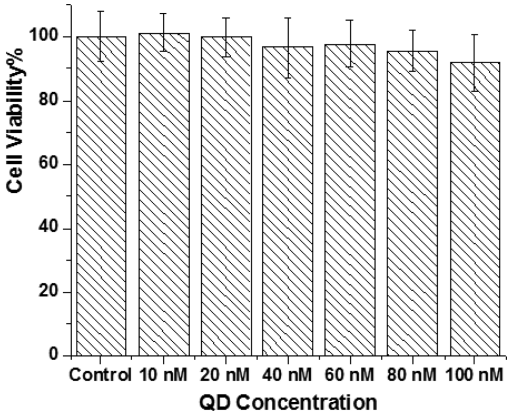

Figure 6. Viability assessment of HeLa cells treated with AB(BC)-QDs at various concentrations for 24 h treatment. Compared to untreated cells (control sample), even at 100 nM (concentration 6X higher than that used in the siRNA delivery experiment), the cell viability is still above 90%.

particle concentrations than the one used in the siRNA delivery experiments (16 nM). Similarly, for RGD-targeted AB(BC)-QDs with enhanced cell uptake, the cytotoxicity was insignificant as well. At concentrations of 40 and 60 nM, the cell viabilities were measured at 98.2 ± 5.4% and 94.3 ± 6.1%, respectively. A couple of factors can help explain this low level of cytotoxicity. First, the positively charged polymer block (PDMA), which often causes toxicity, is partially shielded by the PEG block from direct interaction with cells. Second, the amphiphilic polymers protect QDs from being exposed to the intracellular environment and thus prevent Cd^{2+} release. Indeed, the QDs remain highly fluorescent inside cells, indicating that the core semiconductor QDs are intact during the short time frame of the in vitro experiment. We expect that the long-term biocompatibility can be further improved when more benign nanomaterials are used (e.g., iron oxide nanoparticles).

CONCLUSIONS

Conventionally, DNA and RNA condensations are often achieved by mixing them with cationic polymers (e.g., polyethylenimine and dendrimer) or nanoparticles, which often leads to formation of aggregates above 100 nm. The size of the aggregates is hard to tune to the optimal range for delivery and the size distribution is even more difficult to control. Furthermore, these aggregates exhibit positive surface charges that can result in binding with serum proteins and poor colloidal stability. We have solved these problems by combining inorganic nanoparticles, which serve as both a contrast agent and a structural scaffold, with an rationally designed triblock copolymer that simultaneously realize inorganic nanoparticle solubilization, siRNA condensation, endosome destabilization, and outstanding colloidal stability in complete serum. More importantly, these desired properties are obtained through a simple one-step self-assembly between the nanoparticles and the triblock copolymers, rather than sequentially grafting multiple functional polymers onto nanoparticles. Cell selective delivery of siRNA has also been achieved by linking targeting peptides to the hydrophilic terminus of the block copolymer, without causing significant cytotoxicity. In reference to the original untreated cells, the peptide targeted QD carriers can reduce the target gene expression from ~86 to 25%, whereas the nontargeted control group can only knock down the gene expression to approximately 60% under the same experiment conditions. It is also worth mentioning that semiconductor QDs are used here as a model system because of their unique optical properties and advantages of optical imaging for cellular and small animal studies. Because a variety of inorganic nanoparticles can be made with similar surface properties as QDs,[17−19] we expect this rationally designed triblock copolymer reported

dx.doi.org/10.1021/am3021813 | ACS Appl. Mater. Interfaces 2013, 5, 2845−2852

here can be generalized to encapsulate other nanoparticles for targeted imaging and efficient siRNA delivery.

MATERIALS AND METHODS

Materials. All chemicals were obtained from Sigma-Aldrich (St. Louis, MO) unless otherwise noted. N-octyl methacrylate was purchased from Scientific Polymer Products, Inc. (Ontario, NY). FITC-labeled siRNA, siRNA targeting eGFP, and siRNA of random sequence were obtained from Ambion (Austin, TX). The siRNA sequences targeting eGFP is 5′-GCA AGC UGA CCC UGA AGU UCA U-3′(sense) and 5′-GAA CUU CAG GGU CAG CUU GCC G-3′ (antisense). *cyclo* (Arg-Gly-Asp-D-Phe-Cys) peptide was purchased from Peptides International Inc. (Louisville, Kentucky). Hydrophobic CdSe/ZnS core/shell QDs (620 nm emission) were a gift from Oceannanotech LLC (Springdale, Arkansas, USA). The QDs were received as powders with excess surfactants removed. The dots are coated with hydrophobic surface ligands, trioctylphospine oxide and octadecylamine, and have a quantum efficiency of 50%.

Synthesis of t-Butyl Ester-Terminated AB(BC) Block Copolymer. The triblock copolymer was synthesized via ATRP by monomer addition method using t-butyl 2-bromoisobutyrate as the initiator. In a typical procedure, EGMA monomer (Mn 475 g/mol, 3.6 mmol), initiator (56 uL, 0.3 mmol), and CuCl (30 mg, 0.3 mmol) were added into a Schlenk flask containing butanone (1.8 mL) and isopropyl alcohol (0.45 mL). The flask was sealed with a rubber septum, and degassed via three freeze−pump−thaw cycles, followed by injection of PMDETA (62.8 ul, 0.3 mmol) to start the polymerization in an oil bath preheated at 50 °C. Aliquots were withdrawn at regular time intervals and analyzed by ^{1}H NMR for monitoring the degree of polymerization of EGMA (and also DMA, see below). After 1.5 h, when the EGMA conversion reached ∼95%, degassed DMA monomer (1.75 mL, 10.5 mmol) in 1.5 mL butanone was injected. Further polymerization of 3 h led to DMA monomer conversion of approximately 66%. Lastly, degassed OMA monomer (1.72 mL, 7.8 mmol) in 1.5 mL of butanone solution was added to the flask, and the polymerization was allowed to proceed for 24 h. The polymerization reaction was quenched by immersing the reaction flask into liquid nitrogen and exposing to air. The reaction mixture was diluted with THF and passed through a neutral alumina column to remove the copper catalysts, and the solvent in the mixture was removed by rotary evaporation.

Hydrolysis of the t-Butyl Ester Terminal. After the crude polymer obtained above was dissolved in 15 mL of dioxane, 20 mL of hydrochloric acid (36.5 wt %) was added, and the solution was incubated in an oil bath at 60 °C for 12 h. The hydrolyzed polymer was dialyzed for 48 h to remove impurities. By adjusting the pH of the solution above 10, the polymer was extract by CH_2Cl_2, and dried by anhydrous $MgSO_4$. The solvent was removed by vacuum evaporation. The overall yield of the polymerization reaction was ∼80%. NMR and GPC measurements were conducted to characterize the polymer. GPC analysis showed that the molecular weight (number averaged, Mn) of the polymer is approximately 15 000 with a polydispersity index (PDI) of 1.45.

Preparation and Characterization of AB(BC)-QD. QD was solubilized with the AB(BC) block copolymer via an emulsion procedure. 50 mg AB(BC) copolymer was first dissolved in 6 mL 0.01 M HCl solution. After the pH value of the solution was adjusted to 6.4, QDs (1 mg) suspended in 1 mL $CHCl_3$ were added. The solution mixture was emulsified by a probe sonicator (Misonix XL-2000) and stirred overnight for $CHCl_3$ evaporation. The obtained transparent solution was passed through a 0.22 um filter, and purified by ultracentrifugation to remove excess polymer. The purified water-soluble QDs were characterized for absorption, fluorescence emission, hydrodynamic size, and zeta potential. The lipid-PEG coated QDs as a positive control for colloidally stable nanoparticles were prepared based on previously reported procedures.[29]

cRGD Conjugation. The carboxyl terminal groups on the surface of AB(BC)-QDs (1 nmol, in 1 mL of PBS) were activated with 1-ethyl-3-(3-dimethylaminopropyl) carbodiimide (EDAC, 15 μmol) for 15 min, and the QDs were added to a 4,7,10-Trioxa-1,13-tridecanediamine solution (5 μmol in 1 mL of PBS). The reaction was stirred for 24 h at ambient temperature, and excess 4,7,10-Trioxa-1,13-tridecanediamine was removed by spin filters. The purified AB(BC)-QDs with amine functional groups were activated with sulfo-SMCC cross-linker (20 umol) in PBS buffer for 1h. Excess sulfo-SMCC cross-linker was quickly removed by spin filtering, and the activated QDs with maleimide groups were incubated with the *cyclo* (Arg-Gly-Asp-D-Phe-Cys) peptide (10 umol) in PBS buffer containing 1 mM EDTA for 24 h. Excess peptide molecules were again removed by spin filtering at the end of the reaction. The molecular weight cutoff size of the spin filters was 100k. They were centrifuged at 3600 g for 15 min for QD purification.

Determination of siRNA Loading Capacity of AB(BC)-QD. To determine the binding ratio of siRNA to QDs, FITC-labeled siRNA (20 pmol) was mixed with 10, 4, 2, 1.33, 1, 0.67, and 0.4 pmol of QDs and incubated for 10 min. The complexes were then loaded into agarose gel for electrophoretic analysis to quantify unbound siRNA.

Microscopy and Flow Cytometry Studies of GFP Knockdown in HeLa Cells. GFP-expressing Hela cells were seeded on 24-well plates (50 000 cells/well) in 0.5 mL culture media and allowed to grow at 37 °C in 5% CO_2 for 24 h. The cells were then treated with AB(BC)-QD siRNA complex, RGD-AB(BC)-QD siRNA complex. and Lipofectamine RNAimax siRNA complex (final siRNA concentration 80 nM). The siRNA/QD ratio was kept at 5 for these experiments instead of the saturation value of 15 to ensure sufficient concentration of AB(BC)-QD inside cells to facilitate endosome escape. After 24 h, the cells were washed with fresh growth media and incubated for another 24 h. Fluorescence signals from the QDs and GFP in the treated cells were analyzed with a BD LSR II flow cytometer (∼10 000 live cell events were collected for each sample). For confocal imaging, cells were seeded on dishes with cover glass bottom. Following the same siRNA treatment procedure described for the flow cytometry study, confocal images were obtained using a 63 × oil immersion objective on a Carl Zeiss LSM 510 Meta microscope.

Cytotoxicity Evaluation Using the CellTiter-Blue Assay. Cell viability was assessed with the standard CellTiter-Blue assay. HeLa cells (10 000) were seeded in 96-well plates for 24 h. The cells were treated with the AB(BC)-QD at various concentrations for 24 h and washed with PBS, followed by addition of 20 μL of the CellTiter-Blue reagent. Cell viability was assessed by the absorbance of the converted dye at 570 nm excitation and 590 nm emission on a TECAN Infinite M200 microplate reader.

AUTHOR INFORMATION

Corresponding Author

*E-mail: xgao@u.washington.edu.

Notes

The authors declare no competing financial interest.

■ ACKNOWLEDGMENTS

This work was supported in part by NIH (R01CA140295), NSF (0645080), and the UW Department of Bioengineering. X.H.G. thanks the NSF for a Faculty Early Career Development award (CAREER). We are also grateful to Prof. Suzie Pun for her GFP-expressing HeLa cells, and Dr. Andrew Wang at Oceannanotech for the highly emissive QDs.

■ REFERENCES

(1) Bumcrot, D.; Manoharan, M.; Koteliansky, V.; Sah, D. W. Y. *Nat. Chem. Biol.* **2006**, *2*, 711−719.
(2) Hannon, G. J. *Nature* **2002**, *418*, 244−251.
(3) Scherer, L. J.; Rossi, J. J. *Nat. Biotechnol.* **2003**, *21*, 1457−1465.
(4) Whitehead, K. A.; Langer, R.; Anderson, D. G. *Nat. Rev. Drug Discov.* **2009**, *8*, 129−138.
(5) Zhang, S. B.; Zhao, B.; Jiang, H. M.; Wang, B.; Ma, B. C. *J. Controlled Release* **2007**, *123*, 1−10.
(6) Elbakry, A.; Zaky, A.; Liebkl, R.; Rachel, R.; Goepferich, A.; Breunig, M. *Nano Lett.* **2009**, *9*, 2059−2064.
(7) Lee, J. S.; Green, J. J.; Love, K. T.; Sunshine, J.; Langer, R.; Anderson, D. G. *Nano Lett.* **2009**, *9*, 2402−2406.
(8) Medarova, Z.; Pham, W.; Farrar, C.; Petkova, V.; Moore, A. *Nat. Med.* **2007**, *13*, 372−377.
(9) Xia, T. A.; Kovochich, M.; Liong, M.; Meng, H.; Kabehie, S.; George, S.; Zink, J. I.; Nel, A. E. *ACS Nano* **2009**, *3*, 3273−3286.
(10) Qi, L. F.; Gao, X. H. *ACS Nano* **2008**, *2*, 1403−1410.
(11) Qi, L. F.; Gao, X. H. *Expert Opin. Drug Delivery* **2008**, *5*, 263−267.
(12) Lee, J. H.; Lee, K.; Moon, S. H.; Lee, Y.; Park, T. G.; Cheon, J. *Angew. Chem., Int. Ed.* **2009**, *48*, 4174−4179.
(13) Probst, C. E.; Zrazhevskiy, P.; Bagalkot, V.; Gao, X. H. *Adv. Drug Delivery Rev.* advanced online publication; DOI: 10.1016/j.addr.2012.09.036.
(14) Singh, N.; Agrawal, A.; Leung, A. K. L.; Sharp, P. A.; Bhatia, S. N. *J. Am. Chem. Soc.* **2010**, *132*, 8241−8243.
(15) Zrazhevskiy, P.; Sena, M.; Gao, X. H. *Chem. Soc. Rev.* **2010**, *39*, 4326−4354.
(16) Zrazhevskiy, P.; Gao, X. H. *Nano Today* **2009**, *4*, 414−428.
(17) Park, J.; Lee, E.; Hwang, N.-M.; Kang, M.; Kim, S. C.; Hwang, Y.; Park, J.-G.; Noh, H.-J.; Kim, J.-Y.; Park, J.-H.; Hyeon, T. *Angew. Chem.* **2005**, *117*, 2932−2937.
(18) Jana, N. R.; Peng, X. *J. Am. Chem. Soc.* **2003**, *125*, 14280−14281.
(19) Hu, X. G.; Gao, X. H. *ACS Nano* **2010**, *4*, 6080−6086.
(20) Convertine, A. J.; Benoit, D. S. W.; Duvall, C. L.; Hoffman, A. S.; Stayton, P. S. *J. Controlled Release* **2009**, *133*, 221−229.
(21) Yu, H.; Zou, Y.; Wang, Y.; Huang, X.; Huang, G.; Sumer, B. D.; Boothman, D. A.; Gao, J. *ACS Nano* **2011**, *5*, 9246−9255.
(22) Moghimi, S. M.; Hunter, A. C.; Murray, J. C. *Pharmacol. Rev.* **2001**, *53*, 283−318.
(23) Nel, A. E.; Madler, L.; Velegol, D.; Xia, T.; Hoek, E. M. V.; Somasundaran, P.; Klaessig, F.; Castranova, V.; Thompson, M. *Nat. Mater.* **2009**, *8*, 543−557.
(24) Jiang, W.; KimBetty, Y. S.; Rutka, J. T.; ChanWarren, C. W. *Nat. Nanotechnol.* **2008**, *3*, 145−150.
(25) Cabral, H.; Matsumoto, Y.; Mizuno, K.; Chen, Q.; Murakami, M.; Kimura, M.; Terada, Y.; Kano, M. R.; Miyazono, K.; Uesaka, M.; Nishiyama, N.; Kataoka, K. *Nat. Nanotechnol.* **2011**, *6*, 815−823.
(26) Chen, S. F.; Cao, Z. Q.; Jiang, S. Y. *Biomaterials* **2009**, *30*, 5892−5896.
(27) Owens Iii, D. E.; Peppas, N. A. *Int. J. Pharm.* **2006**, *307*, 93−102.
(28) Tong, S.; Hou, S.; Ren, B.; Zheng, Z.; Bao, G. *Nano Lett.* **2011**, *11*, 3720−3726.
(29) Dubertret, B.; Skourides, P.; Norris, D. J.; Noireaux, V.; Brivanlou, A. H.; Libchaber, A. *Science* **2002**, *298*, 1759−1762.
(30) Pellegrino, T.; Manna, L.; Kudera, S.; Liedl, T.; Koktysh, D.; Rogach, A. L.; Keller, S.; Radler, J.; Natile, G.; Parak, W. J. *Nano Lett.* **2004**, *4*, 703−707.
(31) Lin, C. A. J.; Sperling, R. A.; Li, J. K.; Yang, T. Y.; Li, P. Y.; Zanella, M.; Chang, W. H.; Parak, W. G. J. *Small* **2008**, *4*, 334−341.
(32) Yu, W. W.; Chang, E.; Falkner, J. C.; Zhang, J. Y.; Al-Somali, A. M.; Sayes, C. M.; Johns, J.; Drezek, R.; Colvin, V. L. *J. Am. Chem. Soc.* **2007**, *129*, 2871−2879.
(33) Wu, X. Y.; Liu, H. J.; Liu, J. Q.; Haley, K. N.; Treadway, J. A.; Larson, J. P.; Ge, N. F.; Peale, F.; Bruchez, M. P. *Nat. Biotechnol.* **2003**, *21*, 41−46.
(34) Schabas, G.; Yusuf, H.; Moffitt, M. G.; Sinton, D. *Langmuir* **2008**, *24*, 637−643.
(35) Zhang, F.; Lees, E.; Amin, F.; Gil, P. R.; Yang, F.; Mulvaney, P.; Parak, W. J. *Small* **2011**, *7*, 3113−3127.
(36) Gao, X. H.; Cui, Y. Y.; Levenson, R. M.; Chung, L. W. K.; Nie, S. M. *Nat. Biotechnol.* **2004**, *22*, 969−976.
(37) Wang, M. F.; Felorzabihi, N.; Guerin, G.; Haley, J. C.; Scholes, G. D.; Winnik, M. A. *Macromolecules* **2007**, *40*, 6377−6384.
(38) van Gaal, E. V. B.; Spierenburg, G.; Hennink, W. E.; Crommelin, D. J. A.; Mastrobattista, E. *J. Controlled Release* **2010**, *141*, 328−338.
(39) Davis, M. E. *Mol. Pharmaceutics* **2009**, *6*, 659−668.
(40) Salvador-Morales, C.; Zhang, L.; Langer, R.; Farokhzad, O. C. *Biomaterials* **2009**, *30*, 2231−2240.
(41) Ruoslahti, E.; Pierschbacher, M. D. *Cell* **1986**, *44*, 517−518.
(42) Ruoslahti, E.; Pierschbacher, M. D. *Science* **1987**, *238*, 491−497.
(43) Lim, Y.; Kwon, O. J.; Lee, E.; Kim, P. H.; Yun, C. O.; Lee, M. *Org. Biomol. Chem.* **2008**, *6*, 1944−1948.
(44) Mickler, F. M.; Vachutinsky, Y.; Oba, M.; Miyata, K.; Nishiyama, N.; Kataoka, K.; Brauchle, C.; Ruthardt, N. *J. Controlled Release* **2011**, *156*, 364−373.
(45) Ng, Q. K. T.; Sutton, M. K.; Soonsawad, P.; Xing, L.; Cheng, H.; Segura, T. *Mol. Ther.* **2009**, *17*, 828−836.
(46) Oba, M.; Fukushima, S.; Kanayama, N.; Aoyagi, K.; Nishiyama, N.; Koyama, H.; Kataoka, K. *Bioconjugate Chem.* **2007**, *18*, 1415−1423.